Inorganic Chemistry

Article

pubs.acs.org/IC

Construction of Non-Interpenetrated Charged Metal–Organic Frameworks with Doubly Pillared Layers: Pore Modification and Selective Gas Adsorption

Susan Sen,[†] Subhadip Neogi,[†] Arshad Aijaz,[‡] Qiang Xu,*[,‡] and Parimal K. Bharadwaj*[,†]

[†]Department of Chemistry, Indian Institute of Technology, Kanpur 208016, India

[‡]National Institute of Advanced Industrial Science and Technology (AIST), Ikeda, Osaka 563-8577, Japan

Supporting Information

ABSTRACT: The rigid and angular tetracarboxylic acid 1,3-bis(3,5-dicarboxyphenyl)imidazolium (H_4L^+), incorporating an imidazolium group, has been used with different pyridine-based linkers to construct a series of non-interpenetrated cationic frameworks, $\{[Zn_2(L)(bpy)_2]\cdot(NO_3)\cdot(DMF)_6\cdot(H_2O)_9\}_n$ (**1**), $\{[Zn_2(L)(dpe)_2]\cdot(NO_3)\cdot(DMF)_3\cdot(H_2O)_2\}_n$ (**2**), and $\{[Zn_2(L)(bpb)_2]\cdot(NO_3)\cdot(DMF)_3\cdot(H_2O)_4\}_n$ (**3**) [L = L^{3-}, DMF = *N*,*N*′-dimethylformamide, bpy = 4,4′-bipyridine, dpe = 1,2-di(4-pyridyl) ethylene, bpb = 1,4-bis(4-pyridyl)benzene]. The frameworks consist of $\{[Zn_2(L)]^+\}_n$ two-dimensional layers that are further pillared by the linker ligands to form three-dimensional bipillared-layer porous structures. While the choice of the bent carboxylic acid ligand and formation of double pillars are major factors in achieving charged non-interpenetrated frameworks, lengths of the pillar linkers direct the pore modulation. Accordingly, the N_2 gas adsorption capacity of the activated frameworks (**1a**–**3a**) increases with increasing pillar length. Moreover, variation in the electronic environment and marked difference in the pore sizes of frameworks permit selective CO_2 adsorption over N_2, where **3a** exhibits the highest selectivity. In contrast, the selectivity of CO_2 over CH_4 is reversed and follows the order **1a** > **2a** > **3a**. These results demonstrate that even though the pore sizes of the frameworks are large enough compared to the kinetic diameters of the excluded gas molecules, the electronic environment is crucial for the selective sorption of CO_2.

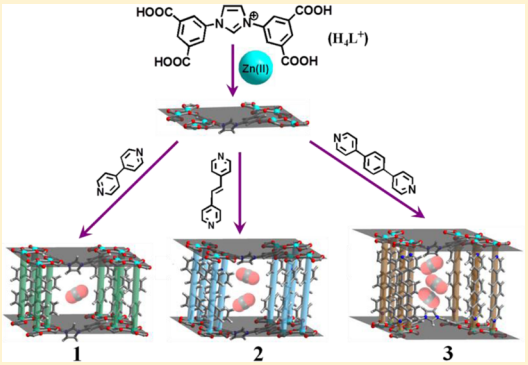

INTRODUCTION

Over the years, porous metal–organic frameworks (MOFs) have been the subject of intense research interest, because of their infinitely ordered structures, high crystallinity, and high porosity, for gas storage,[1] separation,[2] heterogeneous catalysis,[3] sensing,[4] etc.[5] Thus, continuous effort has been devoted to the optimization of the porosity (pore sizes and surface) and stabilities of MOFs, via crystal engineering,[6] for enhanced gas adsorption. Because of the structural fidelity of the building blocks, isoreticular syntheses have been implemented extensively to adjust the pore sizes and shapes by modulating the organic struts.[7] However, the essential prerequisites for instigating permanent porosity in a framework should yield a synthetic protocol that avoids (a) channel clogging, due to excessive framework interpenetration, and (b) channel collapse upon solvent removal.

Among various strategies for constructing three-dimensional (3D) porous MOFs, the "pillar-layer" method is considered one of the most rational and effective ways to design robust 3D porous frameworks.[8] The synthetic protocol promises to generate a wide variety of porous MOF materials;[9] their structures can be predicted through deliberate selection of linker components. Furthermore, mixed coordination (mostly a carboxylate and a N donor) offers ways to control channel functionalization, such as hydrophilic and hydrophobic character, hydrogen bonding, and open metal sites. Thus, mixed ligand metal organic frameworks are likely to display emergent anisotropic, optical, guest transport, and/or other properties.

However, in this *modus operandi*, interpenetration is often inevitable because of the large pore sizes, which decreases the sizes of the overall pore apertures compared to the sizes of those of their non-interpenetrated counterparts.[10] Strategies for controlling MOF interpenetration are, therefore, important and challenging. An interesting approach involves modification of the linker with a bulky pendant arm.[11] Zaworotko and co-workers studied the influence of both reaction temperature and starting material concentration on the extent of subsequent catenation,[12] while Hupp and co-workers achieved the control over catenation via solvent-assisted linker exchange (SALE).[13] A recent report even holds that those metal–carboxylate clusters, containing a double pillar and a double layer, can prevent framework interpenetration[14] in contrast to the single-

Received: April 22, 2014
Published: June 27, 2014

   dx.doi.org/10.1021/ic500900n | *Inorg. Chem.* 2014, 53, 7591–7598

pillar MOFs.[15] However, the strategy for controlling MOF interpenetration by employing (i) a noticeable kink in the carboxylate ligand and (ii) a bipillar unit in the assembly, as we present herein, has not been realized until now.

Bearing in mind the idea that multicarboxylates are good candidates for layer assemblies,[11,16] we used 1,3-bis(3,5-dicarboxyphenyl)imidazolium (H_4L^+) as the ligand (Scheme 1). With Zn(II) ion, this ligand allows the formation of a two-dimensional (2D) layer structure, which is further pillared by a pyridine-based linker ligand to shape the bipillared-layer, 3D MOF. The synthetic strategy allows systematic variation in the length of the pillar ligands to generate open frameworks with tunable window dimensions and pore sizes. Moreover, the presence of an imidazolium moiety in H_4L^+ creates an unusual electropositive environment[17] within the framework that facilitates selective CO_2 adsorption over N_2, at 273 K[18] following the order **1a** < **2a** < **3a**. In contrast, the selectivity of CO_2 over CH_4 is reversed.

Scheme 1. Representation of the Bipillar-Layer Frameworks for the Systematic Modulation of the Pores

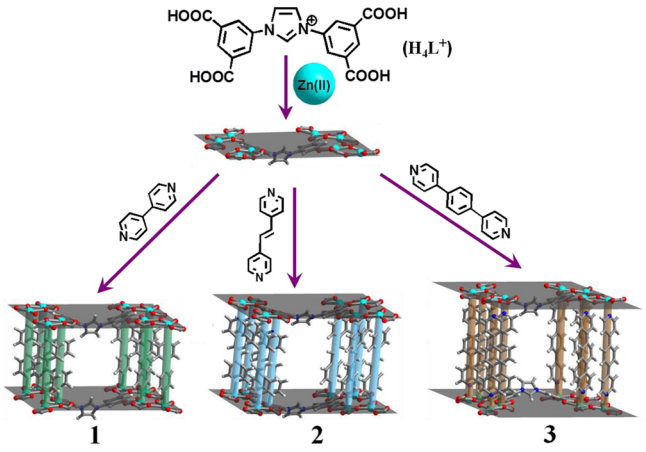

Because CO_2 is currently a tremendous threat in terms of global warming, the development of high-powered carbon capture and sequestration technologies (CCSTs) is imperative for chemistry and material researchers. Selective CO_2 adsorption by MOFs is important for postcombustion capture of CO_2 from flue gas and purification of low-quality natural gas. The significant CO_2 adsorption capacity and selectivity indicate that both the pore size and the electronic environment are crucial parameters in designing frameworks for CO_2 adsorption that can ultimately be useful in the separation of CO_2 from industrial flue gas or natural gas.

EXPERIMENTAL SECTION

Materials and Method. Reagent grade $Zn(NO_3)_2{\cdot}6H_2O$, 4,4′-bipyridine, and 1,2-di(4-pyridyl)ethylene were purchased from Sigma-Aldrich and used without further purification. Ligand dpb was prepared according to a literature procedure,[19] and its purity was checked by nuclear magnetic resonance (NMR) and elemental analysis. All solvents were purified following the established procedures prior to use.

Physical Measurements. Spectroscopic data were collected as follows. IR spectra (KBr disk, 400−4000 cm^{-1}) were recorded on a PerkinElmer model 1320 spectrometer. Powder X-ray diffraction (PXRD) patterns were recorded with a Bruker D8 Advance diffractometer equipped with nickel-filtered Cu Kα radiation. The tube voltage and current were 40 kV and 40 mA, respectively. Microanalyses of the compounds were conducted using a CE-440 elemental analyzer (Exeter Analytical Inc.). Thermogravimetric analyses (TGA) (heating rate of 5 °C/min under a nitrogen atmosphere) were performed with a Mettler Toledo Star System. ^{1}H NMR spectra were recorded on a JEOL JNM-LA500 FT instrument (500 MHz) in DMSO-d_6 with TMS as the internal standard. Melting points were recorded on an electrical melting point apparatus from PERFIT India and are uncorrected. Elemental analyses were conducted by the Central Drug Research Institute (Lucknow, India). Gas adsorption measurements were performed using automatic volumetric BELSORP-MINI-II adsorption equipment. Prior to BET adsorption measurements, as-synthesized compounds were immersed in an ethanol (EtOH) solvent for 3 days at room temperature to replace lattice guest molecules. The solvent-exchanged frameworks were then heated to 100 °C for 12 h under vacuum to produce guest-free compounds **1a**−**3a**.

X-ray Structural Studies. Single-crystal X-ray data were collected at 100 K on a Bruker SMART APEX CCD diffractometer using graphite-monochromated Mo Kα radiation (λ = 0.71069 Å). The linear absorption coefficients, the scattering factors for the atoms, and the anomalous dispersion corrections were taken from International Tables for X-ray Crystallography. Data integration and reduction were conducted with SAINT.[20a] An empirical absorption correction was applied to the collected reflections with SADABS[20b] using XPREP.[20c] The structure was determined by the direct method using SHELXTL[20d] and was refined on F^2 by a full-matrix least-squares technique using the SHELXL-97[20e] program package. The unit cell includes disordered guest anion and solvent molecules, which could not be modeled as discrete atomic sites. Therefore, we employed PLATON/SQUEEZE[21] to calculate the diffraction contribution of solvent molecules and to produce a set of solvent-free diffraction intensities. Structures were then refined again using the data generated. The lattice parameters and structural data are listed in Table S1 of the Supporting Information.

Synthesis of $H_4L^+Cl^-$. Synthesis of the ligand 1,3-bis(3,5-dicarboxyphenyl)imidazolium chloride ($H_4L^+Cl^-$) was achieved in two steps following a slight modification of a literature procedure.[22]

Synthesis of *N*,*N*′-Bis(4-carboxyphenyl)ethylenediimine (A). 5-Aminoisophthalic acid (10 g, 2.0 equiv) was dissolved in dry methanol (30 mL). Formic acid (4 drops) was added followed by dropwise addition of a 30% aqueous solution of glyoxal (4 mL, 1.0 equiv). The solution was stirred at ambient temperature for 24 h. The white solid formed was collected by filtration, washed with cold methanol, and dried in air.

Synthesis of 1,3-Bis(3,5-dicarboxyphenyl)imidazolium Chloride ($H_4L^+Cl^-$). Compound **A** (6 g, 15.62 mmol) was dissolved in anhydrous THF (10 mL) under an argon atmosphere followed by addition of a solution of paraformaldehyde (585 mg, 19.53 mmol, 1.25 equiv) in 12 N HCl (2 mL, 1.5 equiv) in dioxane (4 mL) at 0 °C. The reaction mixture was stirred at room temperature for 4 h. The light pink precipitate formed was collected by filtration, washed with Et_2O, and dried in vacuum: 70% yield; mp >300 °C; ^{1}H NMR (500 MHz, DMSO-d_6, 25 °C, TMS) δ 8.58 (s, 2H, Ar*H*), 8.64 (s, 4H, Ar*H*), 8.73 (d, 2H, Im*H*), 10.68 (s, 1H, Im*H*); ESI-MS m/z 397 (100%) [H_4L^+]. Anal. Calcd for $C_{19}H_{13}N_2O_8Cl$: C, 52.73; H, 3.03; N, 6.47. Found: C, 52.67; H, 3.17; N, 6.36.

Synthesis of 4,4′-(1,4-Phenylene)bispyridine (dpb). The bispyridyl compound was prepared using a modified literature procedure.[23] 4-Bromopyridyl hydrochloride (2.4 g, 17.8 mmol), 1,4-phenyldiboronic acid (1.40 g, 5.92 mmol), and K_2CO_3 (11.6 g, 35.5 mmol) were added to a 2:1:1 PhMe/EtOH/H_2O mixture (300 mL), which had been degassed with argon for 15 min. Next, $Pd(PPh_3)_4$ (0.68 g, 0.59 mmol) was added to the reaction mixture and the solution heated to 120 °C under argon for 48 h. The reaction mixture was then cooled to room temperature and the palladium catalyst filtered off using Celite. The organic phase was concentrated under vacuum and dissolved in CH_2Cl_2, followed by washing with H_2O (three times). Concentrated HCl was added dropwise (pH 2−3) to the organic layer, which caused the desired product to precipitate from solution. The precipitate was collected by filtration and dissolved in

dx.doi.org/10.1021/ic500900n | Inorg. Chem. 2014, 53, 7591−7598

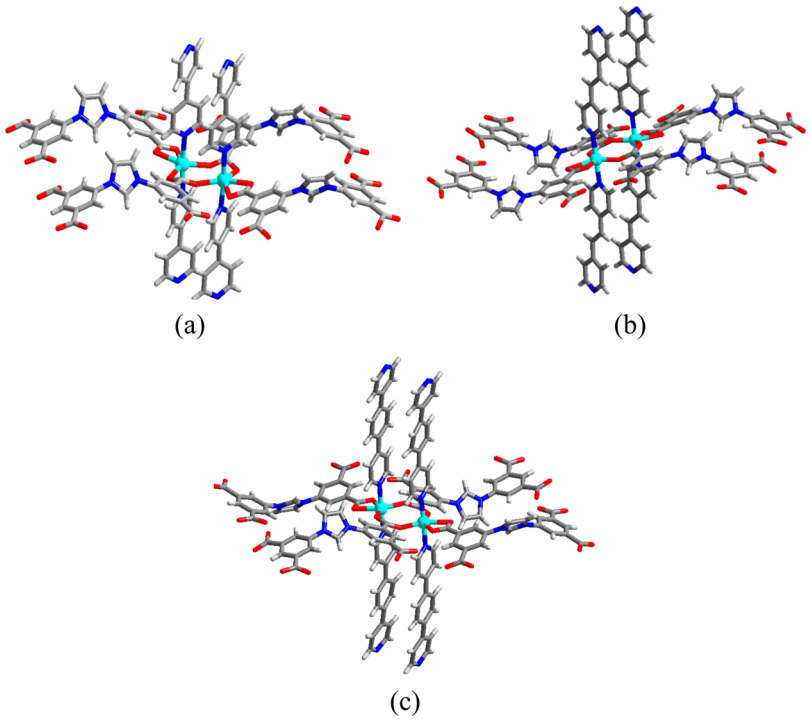

Figure 1. Coordination environment around Zn(II) ions in (a) **1**, (b) **2**, and (c) **3**. Cyan, blue, gray, red, and white spheres represent Zn, N, C, O, and H atoms, respectively.

H_2O. Finally, aqueous NaOH (10 M) was added dropwise to the water layer until the pH was ∼8−9, which resulted in precipitation of the pure product as a white solid: 65% yield; mp 193 °C; ^{1}H NMR (500 MHz, DMSO-d_6, 25 °C, TMS) δ 8.68 (d, 4H, Ar*H*), 7.76 (s, 4H, Ar*H*), 7.54 (d, 2H, Ar*H*); ESI-MS *m*/*z* 233 (100%) [**dpb**]$^+$. Anal. Calcd for $C_{16}H_{12}N_2$: C, 82.73; H, 5.12; N, 12.06. Found: C, 82.68; H, 5.16; N, 11.99.

Synthesis of $\{[Zn_2(L)(bpy)_2]\cdot(NO_3)\cdot(DMF)_6\cdot(H_2O)_9\}_n$ (1). A mixture of $H_4L^+Cl^-$ (30 mg, 0.069 mmol), bpy (10.8 mg, 0.069 mmol), and $Zn(NO_3)_2\cdot 6H_2O$ (82.5 mg, 0.279 mmol) in 3 mL of DMF was sealed in a Teflon-lined stainless steel autoclave and heated under autogenous pressure at 90 °C for 48 h. Cooling to room temperature at a rate of 10 °C/h afforded compound **1** as colorless rectangular parallelopiped crystals in 60% yield: FT-IR (KBr pellets, cm^{-1}) 3419 vs, 3074 w, 1663 vs, 1617 s, 1585 s, 1383 vs, 1218 m, 1099 m, 1073 s, 1014 w, 920 w, 806 m, 778 m, 724 m, 636 s, 489 w. Anal. Calcd for $C_{57}H_{85}N_{13}O_{26}Zn_2$: C, 45.67; H, 5.71; N, 12.15. Found: C, 45.51; H, 5.91; N, 12.03.

Synthesis of $\{[Zn_2(L)(dpe)_2]\cdot(NO_3)\cdot(DMF)_3\cdot(H_2O)_2\}_n$ (2). The synthetic procedure for compound **2** was the same as that for compound **1** except dpe (12.6 mg, 0.069 mmol) was used in place of bpy. Colorless rectangular parallelopiped crystals were isolated in 55% yield: FT-IR (KBr pellet, cm^{-1}) 3418 vs, 3069 w, 1658 m, 1614 s, 1581 s, 1428 s, 1382 vs, 1198 w, 1101 w, 1071 m, 1021 m, 969 w, 829 m, 783 m, 714 w, 665 w, 545 s. Anal. Calcd for $C_{52}H_{54}N_{10}O_{16}Zn_2$: C, 51.8; H, 4.51; N, 11.62. Found: C, 51.64; H, 4.68; N, 11.49.

Synthesis of $\{[Zn_2(L)(bpb)_2]\cdot(NO_3)\cdot(DMF)_3\cdot(H_2O)_4\}_n$ (3). The synthetic procedure for compound **3** was same as that for compound **1** except dpb (16 mg, 0.069 mmol) was used in place of bpy. Colorless rectangular parallelopiped crystals were isolated in 60% yield: FT-IR (KBr pellet, cm^{-1}): 3434 vs, 3060 w, 2935 w, 1656 vs, 1609 s, 1567 s, 1491 m, 1432 m, 1387 s, 1354 m, 1229 m, 1105 m, 1019 m, 814 m, 773 m, 723 s, 582 w, 441 w. Anal. Calcd for $C_{60}H_{52}N_9O_{18}Zn_2$: C, 54.68; H, 3.98; N, 9.57. Found: C, 54.41; H, 4.18; N, 9.32.

RESULTS AND DISCUSSION

The structures of all three isoreticular frameworks were determined by single-crystal X-ray diffraction, which revealed that the fundamental building unit is the same in all cases. This building unit consists of two Zn(II) ions, and each metal exhibits a distorted octahedral coordination geometry with N_2O_4 donor sets. Two pyridyl N atoms from two different linker ligands occupy axial positions. The equatorial positions are occupied by four O atoms from three different L^{3-} (hereafter ***L***) ligand units (Figure 1). Every ligand ***L*** is completely deprotonated and coordinates to six Zn(II) ions through its terminal carboxylate groups, in chelating as well as in μ_2-bridging modes.

The Zn−O bond distances lie in the range of 2.028(15)−2.557(23) Å, and the Zn−N bond distances lie in the range of 2.079(16)−2.276(18) Å, which are comparable to those reported[24] for related complexes. The average Zn(1)···Zn(2) distance (∼4.07 Å) in the dinuclear subunit is almost identical for all the frameworks. These dinuclear units are connected through the long aromatic backbone of the carboxylate ligands to form a cationic 2D layer, $\{[Zn_2(L)]^+\}_n$ (Figure 2), with aperture dimensions of ∼8.6 Å × 7.7 Å. However, the noticeable kink and free rotation of the central imidazolium ring in ***L*** diminish the void of the layer significantly. As a

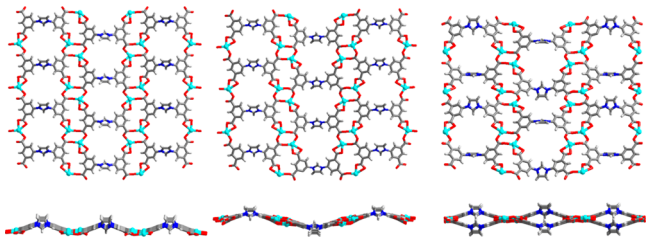

Figure 2. Perspective views of the 2D layer structures in **1**−**3** (from left to right, respectively) along the crystallographic *a*-axis (top) and *c*-axis (bottom). Cyan, blue, gray, red, and white spheres represent Zn, N, C, O, and H atoms, respectively.

dx.doi.org/10.1021/ic500900n | *Inorg. Chem.* 2014, 53, 7591−7598

positive outcome, such layers possibly prevent framework interpenetration, and **1**−**3** are all comprised of single nets.

A comparison of the layer structures of **1**−**3** is shown in Figure 2. Except for the differences (*vide infra*) arising from the different dispositions of the central imidazolium ring of ligand ***L***, such layered motifs are constitutionally similar in **1**−**3** and can be regarded as the platform for the three-dimensional architectures.

Obviously, the 2D layers are not perfectly planar. The free rotation around the C−N bond of the central imidazolium and benzene rings in ***L*** allows deviation from planarity to different extents that can be understood when viewing along the crystallographic *c*-axis (Figure 2, bottom). Furthermore, the obvious twist in the carboxylate ligand directs the imidazolium group to project inside the pore, manifesting an electropositive environment within the framework cavities. The cationic imidazolium ring possesses C_2 symmetry, and only half of the ligand appears in the asymmetric unit. The counter nitrate anion is expected near the imidazolium group but is obscured in the structure. However, the presence of a nitrate anion in all frameworks is confirmed by elemental analyses and further supported by IR spectra (see Figures S4−S6 of the Supporting Information).

The linear N donor linkers (bpy for **1**, dpe for **2**, and bpb for **3**) are coordinated to the axial positions of each Zn(II) ion of the $\{[Zn_2(\boldsymbol{L})]^+\}_n$ layer and extend the resulting framework to a third dimension. Thus, 2D to 3D structural transformation, occurring via linker insertion, generates a series of bipillar-layer structures with 3D interconnected channels (Figure 3). For all the frameworks, strong $\pi-\pi$ stacking interactions exist (range of 3.52−4.03 Å) between the bipillars, which promote the stability and integrity of the framework.

Interestingly, for all the frameworks, with size of a pair of pillaring ligands being essentially larger[8d] than the layer aperture, interpenetration is prevented. More importantly, the structural features of these frameworks (interlayer distances, pore sizes, and free volumes) are exclusively governed by the lengths of the N donor ligands. Accordingly, the calculated guest-accessible area per unit cell volume[25] increases from 3633 Å^3 (∼54.58%) in **1** to 4575 Å^3 (∼58.57%) in **2** to 5079 Å^3 (∼56.99%) in **3**. The values are in ideal correlation with the systematic increase in linker length from bpy (7.06 Å) to dpe (9.36 Å) to bpb (11.29 Å). The increase in the inner cavity space is further reflected in their gas adsorption behavior (*vide infra*).

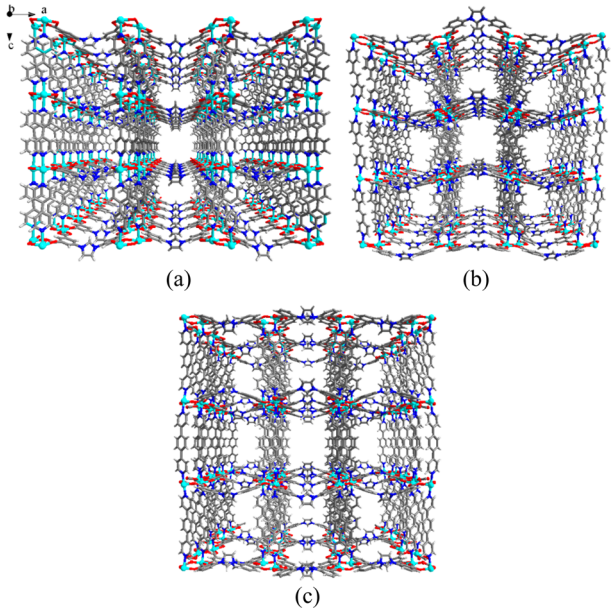

Figure 3. Central projection views of the one-dimensional porous channels in (a) **1**, (b) **2**, and (c) **3** along the crystallographic *b*-axis. Cyan, blue, gray, red, and white spheres represent Zn, N, C, O, and H atoms, respectively.

Although the constructions of non-interpenetrated MOFs **1**−**3** are similar, based on the AA pattern of the 2D layers, some structural difference between them should not be overlooked. While the pillaring ligands in **1**−**3** make approximately right angles with the 2D layer, their increasing length induces noticeable strain in the resulting frameworks. For example, the longest linker bpb in framework **3** exhibits an obvious ∼6° deviation from planarity. This bend leads to sharp twisting in the layer structure also and produces two different kinds of pores along the *c*-axis (Figure 4c and Figure S13 of the Supporting Information).

The cavities of all the metal−organic hosts are occupied by nitrate anions, guest DMF molecules, and water molecules. Although the intrinsic disorder did not allow us to establish all guest molecules unambiguously, the solvent compositions are established from thermogravimetric weight loss and elemental analysis. The total solvent-accessible void volumes of respective frameworks, calculated with PLATON,[21] are in good agreement with the number of guest molecules (3DMF + 4.5H_2O in **1**, 3DMF + 2H_2O in **2**, and 3DMF + 4H_2O in **3**) per asymmetric unit.

Stabilities of 1−3. Thermogravimetric analysis of compound **1** reveals a weight loss of 39.9% (calculated value of 40%) up to 200 °C, corresponding to the loss of lattice DMF and water molecules. The framework is stable up to at least 250 °C (Figure S7 of the Supporting Information). The thermogram of compound **3** shows a weight loss of ∼5.4% (calculated value of 5.5%) up to 120 °C, corresponding to the loss of four lattice water molecules. Further loss of ∼16.8% (calculated value of 16.6%) up to 200 °C corresponds to three lattice DMF molecules. Decomposition of this compound is achieved above 350 °C (Figure S9 of the Supporting Information). Removal of lattice solvent molecules by exchanging with EtOH followed by heating leads to activated compounds **1a** and **3a**. Thermograms of these samples show a plateau up to 250 and 350 °C for **1a** and **3a**, respectively; decomposition starts above these temperatures (Figures S7b and S9b of the Supporting Information). In contrast, TGA of compound **2** reveals a continuous loss of solvent molecules, from room temperature to 150 °C, without a plateau (Figure S8a of the Supporting Information). This behavior reflects the limited thermal stability of framework **2**, which is further verified by VTPXRD patterns. When evacuated, after being exchanged with an EtOH solvent followed by heating, framework **2**, however, shows a flat region in the temperature range of 25−150 °C (Figure S8b of the Supporting Information). To further establish the stability of **1**−**3** toward guest removal, variable-temperature powder X-ray diffraction (VTPXRD) studies were performed for all the frameworks. The VTPXRD studies for **1** and **3** divulge that the crystallinity and overall framework integrity are maintained up to 200 °C, while framework **2** sustains the framework integrity up to 150 °C (Figures S10−S12 of the Supporting Information). This information is helpful during activation of the frameworks for gas adsorption experiments.

dx.doi.org/10.1021/ic500900n | *Inorg. Chem.* 2014, 53, 7591−7598

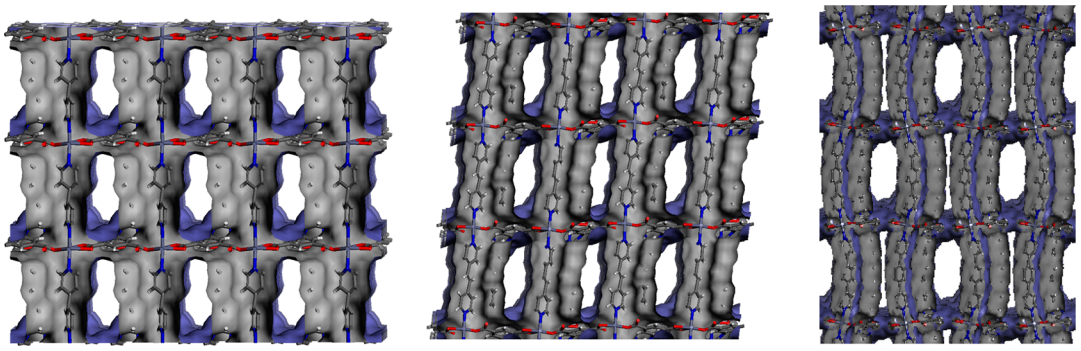

Figure 4. Views of isoreticular MOFs [(a) **1**, (b) **2**, and (c) **3**] along the *c*-axis. The gradual increase in pore size, using the augmented length of the pillar ligand, is exemplified.

Gas Adsorption Studies. The controlled increase in the pore size of the MOFs, together with their robust nature and the presence of 3D channels (Figure 4 and Figure S14 of the Supporting Information), satisfies the essential prerequisites for gas sorption measurements. To this end, gas adsorption studies were conducted up to a relative pressure (p/p_0) of 1.0 on the activated frameworks at STP. Activation of samples involved the exchange of solvent molecules with EtOH, followed by vacuum drying at 100 °C for 12 h. The N_2 sorption isotherms at 77 K for all the compounds show a typical type I behavior (Figure 5) without any hysteresis. The sorption of nitrogen at

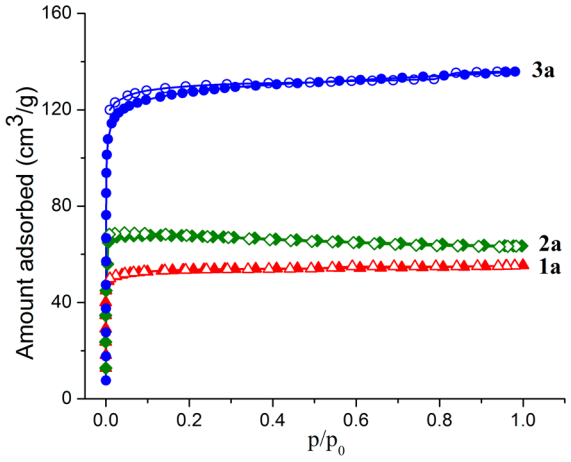

Figure 5. Nitrogen adsorption isotherms of **1a**−**3a** at 77 K [adsorption and desorption for **1a** (▲ and △, respectively), **2a** (◆ and ◇, respectively), and **3a** (● and ○, respectively)].

77 K reaches near saturation at low relative pressures (p/p_0 < 0.02) and thereafter increases very slowly up to 1 atm, indicating the microporous nature of the frameworks. The total gas uptakes of **1a**−**3a** are 55.4, 68.1, and 135.9 cm^3/g, respectively, with related Brunauer−Emmette−Teller (BET) surface areas 181, 235, and 425 m^2/g, respectively. Clearly, the N_2 adsorption capacity decreases in following order: **3a** > **2a** > **1a**. This is in full agreement with the increasing length of the pillar linkers. The pore sizes of the frameworks, as calculated from N_2 sorption studies, are found to be 0.61 nm for **1a**, 0.63 nm for **2a**, and 0.66 nm for **3a** (Figures S15−S17 of the Supporting Information). However, it is worth pointing that in spite of the great difference in the void volume between **1** and **2**, the N_2 sorption study reveals almost comparable uptake for both activated frameworks. This inconsistency can be correlated with the low thermal stability of **2** toward desolvation, as monitored via TGA and VPXRD studies.

The microporous nature and charged frameworks prompted us further to explore their CO_2 capture and separation properties. The sorption isotherms of CO_2 at 195, 273, and 298 K for the activated frameworks are probed up to a relative pressure (p/p_0) of 1.0 at STP. To our appreciation, the maximal CO_2 uptakes at 298, 273, and 195 K for **1a** are 14.7, 33.9, and 50.6 cm^3/g, respectively. For **2a** and **3a**, these values are 26.8, 35.5, and 74.9 cm^3/g and 34.4, 54.3, and 146.9 cm^3/g, respectively (Figure 6). The aforementioned numbers indicate a systematic increase in the uptake capacity, consistent with the order of pore size. For all the activated frameworks, the curves show a rapid CO_2 uptake in the initial stage, implying favorable interaction between CO_2 molecules and the host framework (*vide infra*). Evidently, the CO_2 uptake values are reasonably high for all the frameworks and comparable with those of recently reported frameworks.[26]

To gain more insight into the interaction of the adsorbate with the framework, the isosteric heat of CO_2 adsorption (Q_{st}) for the activated frameworks is evaluated utilizing the Clausius−Clayperon equation,[27] from the isotherms obtained at 273 and 298 K. As depicted in Figure 7, the Q_{st} value (in kilojoules per mole) at zero coverage reaches 36.0 for **1a**, 20.4 for **2a**, and 23.5 for **3a** and shows steady retention at higher coverages. The results signify that under the low-pressure measurement condition, the narrow pore size of **1a** facilitates the optimization of the CO_2−framework and adsorbant−adsorbant interactions. However, in the case of **2a** and **3a**, the values are low and comparable because of their larger pore sizes. Also, the slightly lower Q_{st} of **2a** may be attributed to the partial collapse of the framework.

To further establish the potential properties of the activated frameworks with respect to gas separation, their selective CO_2 capture abilities over N_2 and CH_4 gases are probed at 273 K. Figure 8 shows that N_2 molecules, because of their low polarizability and high thermal energy, do not diffuse into the channels of any framework. The CO_2 selectivities over N_2 for **1a**, **2a**, and **3a** are calculated as described previously[24] and found to be 40, 113, and 181, respectively. To the best of our knowledge, such a high CO_2 selectivity over N_2, as observed for **3a**, is rarely reported and among the excellent CO_2 selectivity values in MOFs[28] reported to date.

It is worth mentioning that the CO_2/N_2 adsorption amount ratios at 0.16 atm[29] (typical partial pressure of CO_2 in industrial

dx.doi.org/10.1021/ic500900n | Inorg. Chem. 2014, 53, 7591−7598

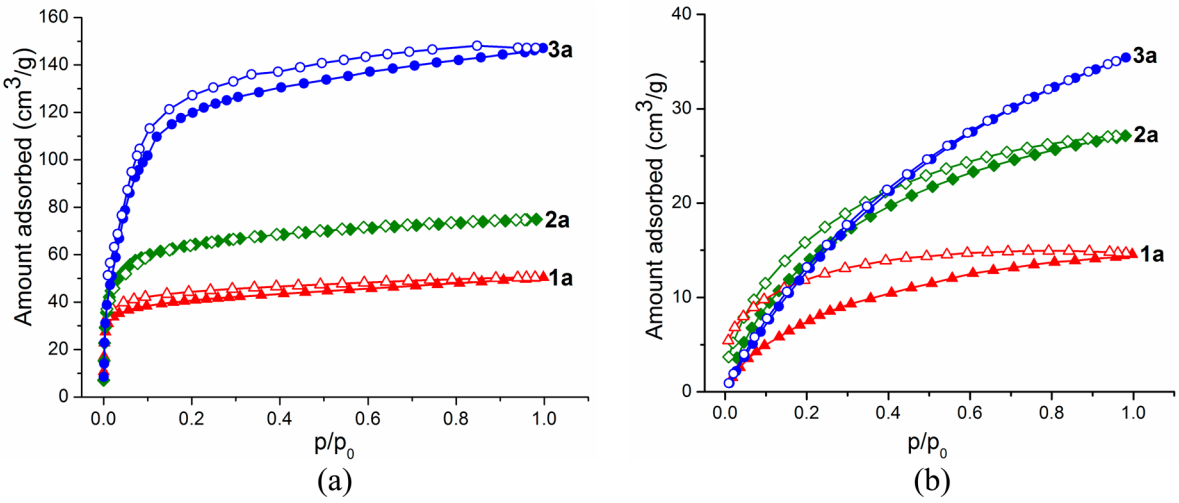

Figure 6. (a) Carbon dioxide adsorption isotherms of **1a**–**3a** at 195 K. (b) CO_2 adsorption isotherms at 298 K [adsorption and desorption for **1a** (▲ and △, respectively), **2a** (◆ and ◇, respectively), and **3a** (● and ○, respectively)].

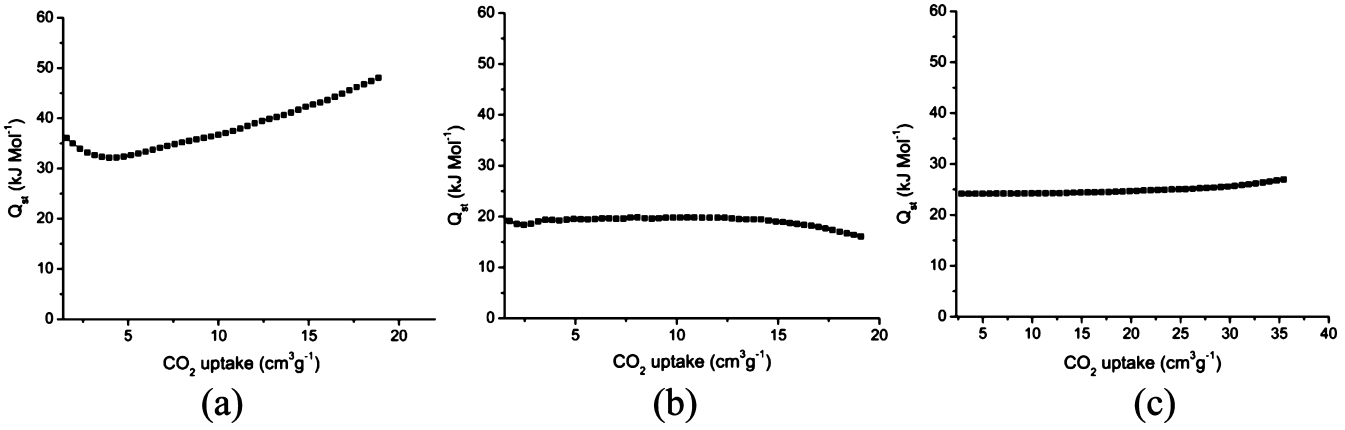

Figure 7. Isosteric heats of CO_2 adsorption (Q_{st}) for (a) **1a**, (b) **2a**, and (c) **3a**.

flue gas) for **1a**–**3a** equal 47, 36, and 234, respectively. To our delight, the value for **3a** is comparable even with the best values recently reported for MOFs[30] under similar measurement conditions. The excellent CO_2 adsorption selectivity and capacity suggest that **3a** may find potential applications in the separation of CO_2 from industrial flue gas. On the basis of the aforementioned results, we reasoned that the contributing factors for these selectivities include[25] the presence of the exposed imidazolium moieties and counterions and accessibility of electron rich double-pillar linkers. These three features generate a polar cavity that preferentially adsorbs CO_2 because of its high quadrupole moment and polarizability (13.4×10^{-40} C m^2 and 26.3×10^{-25} cm^3, respectively).[31] However, it should be noted that the CO_2 adsorption–desorption curve at 273 K (Figure 8) shows strong hysteresis for **1a** and **2a**. While this behavior for **1a** can be correlated with rather slow kinetics, instigated by the strong CO_2–framework interaction (*vide supra*), we assume that the hysteretic curve in the case of **2a** is a result of partial framework collapse during the desorption process. For both **1a** and **3a**, the adsorption–desorption experiments were conducted several times and produced the same result. In the case of **2a**, however, the reproducibility was poor after two cycles.

Further interesting results are obtained for CH_4 adsorption at 273 K. The CH_4 uptake values at 1 bar for **1a**–**3a** are 3.3, 7.5, and 25.6 cm^3/g, respectively. Clearly, **1a** adsorbs the least CH_4 in the given pressure range. Although CH_4 has a kinetic diameter (3.8 Å) larger than that of N_2 (3.64 Å), favorable adsorption of the former in **3a** can be correlated with the polarizability of CH_4 (26×10^{-25} cm^3) that is larger than that of N_2 (17.6×10^{-25} cm^3). Thus, the availability of π-electron rich benzene spacers in the pillar linker facilitates the interaction of CH_4 molecules with the framework wall and adsorption. As a consequence, the CO_2 selectivities over CH_4 for **1a**–**3a** at 273 K calculated as described previously[24] are found to be 48.3, 16.5, and 4.2, respectively. Considering the aforementioned outcome, **1a** exhibits the highest CO_2 versus CH_4 selectivity among all three frameworks, and the value is also remarkably superior to those of other reported MOFs.[26,32]

CONCLUSION

In conclusion, use of 1,3-bis(3,5-dicarboxyphenyl)imidazolium (H_4L^+) ligand with Zn(II) ion allows the formation of a 2D layer structure, which is further pillared by pyridine-based linkers in the construction of non-interpenetrated and charged metal–organic frameworks with doubly pillared layers. The pillaring roles of the rigid bipyridyl linkers are imperative and diverse, as they not only fix the neighboring 2D layers with an appropriate distance and prevent the clogging of micropores but also adjust the pore size of the frameworks. Accordingly,

dx.doi.org/10.1021/ic500900n | Inorg. Chem. 2014, 53, 7591–7598

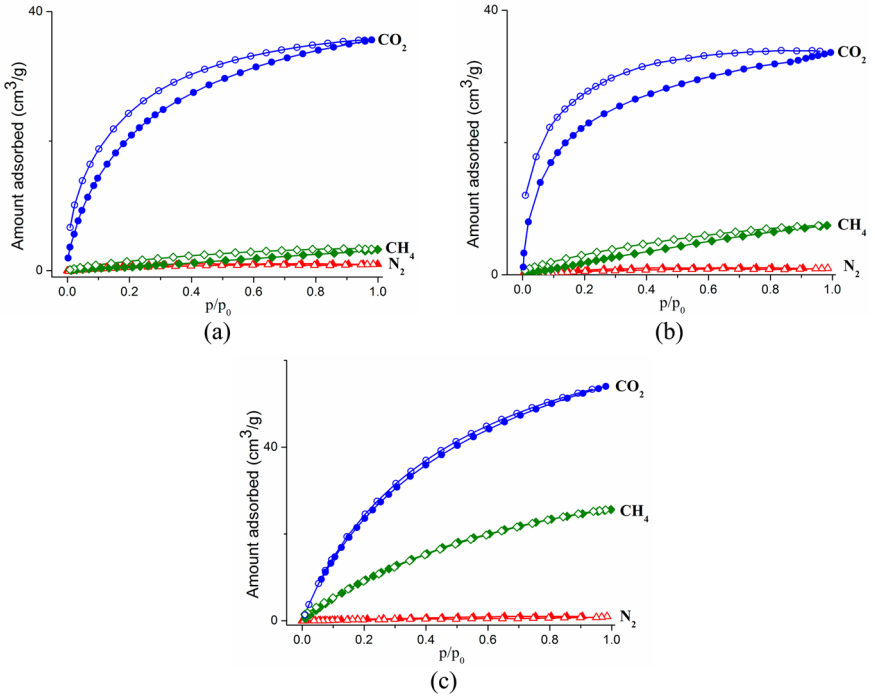

Figure 8. CO_2, N_2, and CH_4 physisorption isotherms of activated (a) **1a**, (b) **2a**, and (c) **3a** at 273 K [adsorption and desorption of N_2 (▲ and △, respectively), adsorption and desorption of CH_4 (◆ and ◇, respectively), and adsorption and desorption of CO_2 (● and ○, respectively)].

the change in the length of the pillared ligands becomes an effective strategy for modulating the pore size and adsorption properties. The N_2 adsorption studies of the activated frameworks follow the gradual increase in capacity with an increase in pillar length. Moreover, the presence of the exposed imidazolium moieties and counterions and the accessibility to electron rich double-pillar linkers permit easy discrimination of CO_2 over N_2, following the order **1a** < **2a** < **3a**. On the other hand, the framework selectivity of CO_2 over CH_4 is just reversed. The sorption results allow us to conclude that although the pore sizes of the frameworks are large enough compared to the kinetic diameters of N_2 and CH_4, the electronic environment plays a pivotal role in the selective sorption of CO_2 over other gas molecules. While the excellent CO_2 selectivity over N_2 for **3a** is among the best values published to date, **1a** exhibits CO_2 versus CH_4 selectivity that is superior to those of the commonly reported MOFs. Overall, the results present a novel design principle of charged, non-interpenetrated, pillared-layer MOFs for tuning the selective ability, for possible applications in the separation of CO_2 from flue gas or natural gas mixtures.

■ ASSOCIATED CONTENT

Ⓢ Supporting Information

Several spectroscopic, thermogravimetric analysis, and powder X-ray diffraction patterns of compounds **1**−**3**, a table that includes X-ray crystallographic data, and figures. This material is available free of charge via the Internet at http://pubs.acs.org.

■ AUTHOR INFORMATION

Corresponding Authors

*E-mail: q.xu@aist.go.jp. Fax: (+81) 72-751-7942. Telephone: (+81) 72-751-9562.

*E-mail: pkb@iitk.ac.in. Fax: (+91) 512-259-7436. Telephone: (+91) 512-259-7034.

Notes

The authors declare no competing financial interest.

■ ACKNOWLEDGMENTS

We gratefully acknowledge the financial support from the Department of Science and Technology, New Delhi, India (J. C. Bose National Fellowship to P.K.B.). S.N. thanks IIT Kanpur for a postdoctoral fellowship.

■ REFERENCES

(1) (a) Cheon, Y. E.; Suh, M. P. *Chem. Commun.* **2009**, 2296−2298. (b) Kanoo, P.; Matsuda, R.; Higuchi, M.; Kitagawa, S.; Maji, T. K. *Chem. Mater.* **2009**, *21*, 5860−5866.

(2) (a) Kosal, M. E.; Chou, J.-H.; Wilson, S. R.; Suslick, K. S. *Nat. Mater.* **2002**, *1*, 118−121. (b) Kondo, M.; Okubo, T.; Asami, A.; Noro, S.-I.; Yoshitomi, T.; Kitagawa, S.; Ishii, T.; Matsuzaka, H.; Seki, K. *Angew. Chem., Int. Ed.* **1999**, *38*, 140−143. (c) Zhang, Z.; Zhao, Y.; Gong, Q.; Lib, Z.; Li, J. *Chem. Commun.* **2013**, *49*, 653−661. (d) Nagarkar, S. S.; Chaudhuri, A. K.; Ghosh, S. K. *Inorg. Chem.* **2012**, *51*, 572−576. (e) Keksin, S.; van Heest, T. M.; Sholl, D. S. *ChemSusChem* **2010**, *3*, 879−891.

(3) (a) Fujita, M.; Kwon, Y. J.; Washizu, S.; Ogura, K. *J. Am. Chem. Soc.* **1994**, *116*, 1151−1152. (b) Wu, C. D.; Hu, A.; Zhang, L.; Lin, W. *J. Am. Chem. Soc.* **2005**, *127*, 8940−8941. (c) Dybtsev, D. N.; Nuzhdin, A. L.; Chun, H.; Bryliakov, K. P.; Talsi, E. P.; Fedin, V. P.; Kim, K. *Angew. Chem., Int. Ed.* **2006**, *45*, 916−920. (d) Uemura, T.; Kitaura, R.; Ohta, Y.; Nagaoka, M.; Kitagawa, S. *Angew. Chem., Int. Ed.* **2006**, *45*, 4112−4116.

(4) (a) Mir, M. H.; Koh, L. L.; Tan, G. K.; Vittal, J. J. *Angew. Chem., Int. Ed.* **2010**, *49*, 390−393. (b) Zeller, M. *Inorg. Chem.* **2008**, *47*, 5122−5128. (c) Lipkowski, J. In *Inclusion Compounds*; Atwood, J. L., Davies, J. E. D., MacNicol, D. D., Eds.; Academic Press: New York, 1984; Vol. *1*, pp 59.

(5) (a) Kitagawa, S.; Kitaura, R.; Noro, S. *Angew. Chem., Int. Ed.* **2004**, *43*, 2334−2375. (b) Long, J. R.; Yaghi, O. M. *Chem. Soc. Rev.* **2009**, *38*, 1213−1214. (c) Sculley, J.; Yuan, D.; Zhou, H.-C. *Energy Environ. Sci.* **2011**, *4*, 2721−2735. (d) Zhang, J.-P.; Zhang, Y.-B.; Lin, J.-B.; Chen, X.-M. *Chem. Rev.* **2012**, *112*, 1001−1033.

(6) (a) Moulton, B.; Zaworotko, M. J. *Chem. Rev.* **2001**, *101*, 1629−1658. (b) Delgado-Friedrichs, O.; O'Keeffe, M.; Yaghi, O. M. *Phys. Chem. Chem. Phys.* **2007**, *9*, 1035−1043.
(7) (a) Lin, X.; Telepeni, I.; Blake, A. J.; Dailly, A.; Brown, C. M.; Simmons, J. M.; Zoppi, M.; Walker, G. S.; Thomas, K. M.; Mays, T. J.; Hubberstey, P.; Champness, N. R.; Schroder, M. J. *J. Am. Chem. Soc.* **2009**, *131*, 2159−2171. (b) Yuan, D. Q.; Zhao, D.; Sun, D. F.; Zhou, H.-C. *Angew. Chem., Int. Ed.* **2010**, *49*, 5357−5361. (c) Furukawa, H.; Ko, N.; Go, Y. B.; Aratani, N.; Choi, S. B.; Choi, E.; Yazaydin, A. O.; Snurr, R. Q.; O'Keeffe, M.; Kim, J.; Yaghi, O. M. *Science* **2010**, *329*, 424−428.
(8) (a) Wang, R.; Hong, M.; Yuan, D.; Sun, Y.; Xu, L.; Luo, J.; Cao, R.; Chan, A. S. C. *Eur. J. Inorg. Chem.* **2004**, 37−43. (b) Kitaura, R.; Lwahori, F.; Matsuda, R.; Kitagawa, S.; Kubota, Y.; Takata, M.; Kobayashi, T. C. *Inorg. Chem.* **2004**, *43*, 6522−6524. (c) Pan, L.; Liu, H.; Kelly, S. P.; Huang, X.; Olson, D. H.; Li, J. *Chem. Commum.* **2003**, 854−855. (d) Wang, X.-F.; Zhang, Y.-B.; Xue, W. *Cryst. Growth Des.* **2012**, *12*, 1626−1631.
(9) (a) Park, J.; Li, J.-R.; Sanudo, E. C.; Yuan, D.; Zhou, H.-C. *Chem. Commun.* **2012**, *48*, 883−885. (b) Chen, Q.; Lin, J.-B.; Xue, W.; Zeng, M.-H.; Chen, X.-M. *Inorg. Chem.* **2011**, *50*, 2321−2328. (c) Xiang, S.-C.; Zhang, Z.; Zhao, C.-G.; Hong, K.; Zhao, X.; Ding, D.-R.; Xie, M.-H.; Wu, C.-D.; Das, M. C.; Gill, R.; Thomas, K. M.; Chen, B. *Nat. Commun.* **2011**, *2*, 204−209.
(10) Kim, H.; Das, S.; Kim, M. G.; Dybtsev, D. N.; Kim, Y.; Kim, K. *Inorg. Chem.* **2011**, *50*, 3691−3696.
(11) Farha, O. K.; Malliakas, C. D.; Kanatzidis, M. G.; Hupp, J. T. *J. Am. Chem. Soc.* **2010**, *132*, 950−952.
(12) Zhang, J. J.; Wojtas, L.; Larsen, R. W.; Eddaoudi, M.; Zaworotko, M. J. *J. Am. Chem. Soc.* **2009**, *131*, 17040−17041.
(13) Bury, W.; Fairen-Jimenez, D.; Lalonde, M. B.; Snurr, R. Q.; Farha, O. K.; Hupp, J. T. *Chem. Mater.* **2013**, *25*, 739−744.
(14) Zeng, M.-H.; Wang, Q.-X.; Tan, Y.-X.; Hu, S.; Zhao, H.-X.; Long, L.-S.; Kurmoo, M. J. *J. Am. Chem. Soc.* **2010**, *132*, 2561−2563.
(15) (a) Ma, B.-Q.; Mulfort, K. L.; Hupp, J. T. *Inorg. Chem.* **2005**, *44*, 4912−4914. (b) Jia, J.; Lin, X.; Wilson, C.; Blake, A. J.; Champness, N. R.; Hubberstey, P.; Walker, G.; Cussen, E. J.; Schroder, M. *Chem. Commun.* **2007**, 840−842. (c) Zhang, Y. B.; Zhang, W. X.; Feng, F. Y.; Zhang, J. P.; Chen, X. M. *Angew. Chem., Int. Ed.* **2009**, *48*, 5287−5290.
(16) (a) Choi, E.-Y.; Wray, C. A.; Hu, C.; Choe, W. *CrystEngComm* **2009**, *11*, 553−555. (b) Burnett, B. J.; Barron, P. M.; Hu, C.; Choe, W. *J. Am. Chem. Soc.* **2011**, *133*, 9984−9987.
(17) (a) Sen, S.; Nair, N. N.; Yamada, T.; Kitagawa, H.; Bharadwaj, P. K. *J. Am. Chem. Soc.* **2012**, *134*, 19432−19437. (b) Piecha, A.; Gągor, A.; Jakubas, R.; Szklarz, P. *CrystEngComm* **2013**, *15*, 940−944. (c) Lee, J. Y.; Roberts, J. M.; Farha, O. K.; Sarjeant, A. A.; Scheidt, K. A.; Hupp, J. T. *Inorg. Chem.* **2009**, *48*, 9971−9973. (d) Sen, S.; Yamada, T.; Kitagawa, H.; Bharadwaj, P. K. *Cryst. Growth Des.* **2014**, *14*, 1240−1244.
(18) (a) Vaidhyanathan, R.; Iremonger, S. S.; Dawson, K. W.; Shimizu, G. K. H. *Chem. Commun.* **2009**, 5230−5232. (b) Vaidhyanathan, R.; Iremonger, S. S.; Shimizu, G. K. H.; Boyd, P. G.; Alavi, S.; Woo, T. K. *Science* **2010**, *330*, 650−653. (c) Inubushi, Y.; Horika, S.; Fukushima, T.; Akiyama, G.; Matsuda, R.; Kitagawa, S. *Chem. Commun.* **2010**, *46*, 9229−9231.
(19) Xue, M.; Ma, S.; Jin, Z.; Schaffino, R. M.; Zhu, G.-S.; Lobkovsky, E. B.; Qiu, S.-L.; Chen, B. *Inorg. Chem.* **2008**, *47*, 6825−6828.
(20) (a) *SAINT+*, version 6.02; Bruker AXS: Madison, WI, 1999. (b) Sheldrick, G. M. *SADABS, Empirical Absorption Correction Program*; University of Göttingen: Göttingen, Germany, 1997. (c) *XPREP*, version 5.1; Siemens Industrial Automation Inc.: Madison, WI, 1995. (d) Sheldrick, G. M. *SHELXTL Reference Manual*, version 5.1; Bruker AXS: Madison, WI, 1997. (e) Sheldrick, G. M. *SHELXL-97, Program for Crystal Structure Refinement*; University of Göttingen: Göttingen, Germany, 1997.
(21) Spek, A. L. *J. Appl. Crystallogr.* **2003**, *36*, 7−13.
(22) Suessner, M.; Plenio, H. *Chem. Commun.* **2005**, *43*, 5417−5419.
(23) Amoroso, A. J.; Thompson, A. M. W. C.; Maher, J. P.; McCleverty, J. A.; Ward, M. D. *Inorg. Chem.* **1995**, *34*, 4828−4835.
(24) Sen, S.; Neogi, S.; Aijaz, A.; Xu, Q.; Bharadwaj, P. K. *Dalton Trans.* **2014**, *43*, 6100−6107.
(25) Calculated using PLATON and after deducting the area for the unlocated nitrate anion in the cavity.
(26) (a) Rowsell, J. L. C.; Millward, A. R.; Park, K. S.; Yaghi, O. M. *J. Am. Chem. Soc.* **2004**, *126*, 5666−5667. (b) Banerjee, R.; Furukawa, H.; Britt, D.; Knobler, C.; O'Keeffe, M.; Yaghi, O. M. *J. Am. Chem. Soc.* **2009**, *131*, 3875−3877.
(27) Kaye, S. S.; Long, J. R. *J. Am. Chem. Soc.* **2005**, *127*, 6506−6507.
(28) (a) Li, C.-P.; Du, M. *Chem. Commun.* **2011**, *47*, 5958−5972. (b) Hou, L.; Shi, W.-J.; Wang, Y.-Y.; Guo, Y.; Jin, C.; Shi, Q.-Z. *Chem. Commun.* **2011**, *47*, 5464−5466. (c) Chen, S.-S.; Chen, M.; Takamizawa, S.; Chen, M.-S.; Su, Z.; Sun, W.-Y. *Chem. Commun.* **2011**, *47*, 752−754. (d) Ortiz, G.; Brandès, S.; Rousselin, Y.; Guilard, R. *Chem.—Eur. J.* **2011**, *17*, 6689−6695.
(29) Liu, B.; Hou, L.; Wang, Y.-Y.; Miao, H.; Bao, L.; Shi, Q.-Z. *Dalton Trans.* **2012**, *41*, 3209−3213.
(30) (a) Choi, H. S.; Suh, M. P. *Angew. Chem., Int. Ed.* **2009**, *48*, 6865−6869. (b) Zhang, J.; Wu, H.; Emge, T. J.; Li, J. *Chem. Commun.* **2010**, *46*, 9152−9154. (c) Caskey, S. R.; Wong-Foy, A. G.; Matzger, A. *J. Am. Chem. Soc.* **2008**, *130*, 10870−10871.
(31) Mason, J. A.; Sumida, K.; Herm, Z. R.; Krishna, R.; Long, J. R. *Energy Environ. Sci.* **2011**, *4*, 3030−3040.
(32) (a) Saha, D.; Bao, Z.; Jia, F.; Deng, S. *Environ. Sci. Technol.* **2010**, *44*, 1820−1826. (b) Zheng, B.; Bai, J.; Duan, J.; Wojtas, L.; Zaworotko, M. J. *J. Am. Chem. Soc.* **2011**, *133*, 748−751. (c) Li, H.; Shi, W.; Zhao, K.; Niu, Z.; Li, H.; Cheng, P. *Chem.—Eur. J.* **2013**, *19*, 3358−3365.